JGR Atmospheres

RESEARCH ARTICLE
10.1029/2025JD044010

Climatology of Cloud-Land-Surface Coupling Across Different ARM Sites

Natalia Roldán-Henao[1], Tianning Su[1,2], Zhanqing Li[1], Youtong Zheng[3,4], and John Yorks[5]

[1]Department of Atmospheric and Oceanic Sciences and ESSIC, University of Maryland, College Park, MD, USA, [2]Lawrence Livermore National Laboratory, Livermore, CA, USA, [3]Department of Earth and Atmospheric Science, University of Houston, Houston, TX, USA, [4]Institute of Climate and Atmospheric Science, University of Houston, Houston, TX, USA, [5]NASA Goddard Space Flight Center, Greenbelt, MD, USA

Key Points:

- This study performs a climatology of cloud-surface coupling in five countries across three continents
- Our method examines heat fluxes, thermodynamic profiles, and vertical velocity for coupled and decoupled clouds
- We observed consistent coupling threshold and percentage across diverse landscapes

Supporting Information:

Supporting Information may be found in the online version of this article.

Correspondence to:

Z. Li,
zhanqing@umd.edu

Citation:

Roldán-Henao, N., Su, T., Li, Z., Zheng, Y., & Yorks, J. (2026). Climatology of cloud-land-surface coupling across different ARM sites. *Journal of Geophysical Research: Atmospheres*, *131*, e2025JD044010. https://doi.org/10.1029/2025JD044010

Received 31 MAR 2025
Accepted 8 DEC 2025

Author Contributions:

Conceptualization: Natalia Roldán-Henao, Tianning Su, Youtong Zheng
Data curation: Natalia Roldán-Henao
Formal analysis: Natalia Roldán-Henao
Funding acquisition: Zhanqing Li, John Yorks
Investigation: Natalia Roldán-Henao, Youtong Zheng, John Yorks
Methodology: Natalia Roldán-Henao, Tianning Su
Project administration: Zhanqing Li
Resources: Zhanqing Li
Software: Natalia Roldán-Henao
Supervision: Zhanqing Li, John Yorks
Validation: Natalia Roldán-Henao, Tianning Su
Writing – original draft: Natalia Roldán-Henao

Abstract Land-atmosphere interactions play a critical role in the evolution and formation of low-level clouds. The different states of coupling between low-level clouds and the surface are uncertain, primarily over continental regions, where complex thermodynamics complicates their investigation. This study uses observations from the Atmospheric Radiation Measurement User Facility to explore cloud-surface coupling and perform a climatological analysis of this interaction in five countries across three continents. The results reveal consistent coupling thresholds and average percentages across the five sites, with coupled clouds accounting for 66% of the cases and decoupled clouds for 34%. Thermodynamic and dynamic evaluations show distinct differences between coupled and decoupled clouds. Coupled clouds are characterized by humid environments, in which vertical motions connect the surface and lower atmosphere to the cloud base, conditions that favor the formation of boundary layer clouds. Decoupled clouds prefer to occur in a drier and colder environment with vertical motions inside the boundary layer being detached from the cloud base, under which boundary layer clouds are hard to form. Coupled clouds peak during warmer hours and seasons, and vice versa for decoupled clouds. This study underscores the complexity of cloud-land-surface interactions and paves the way for further investigations into cloud formation and evolution under different atmospheric environments.

Plain Language Summary The Earth's surface serves as a source of heat, moisture, momentum, and various atmospheric elements. The interaction between the Earth's fluxes and the atmosphere not only alters the properties and development of the atmosphere itself but also affects the characteristics of clouds situated in or near the first atmospheric layer, known as the planetary boundary layer. This study assesses the relationship between the Earth's surface and low-level clouds using a comprehensive set of ground-based observational data collected from five Department of Energy Atmospheric Radiation Measurement User Facilities. Our findings indicate that the proportion of coupled to decoupled clouds is similar across different landscapes, with an average of 66% of the clouds being coupled and 34% decoupled. We observed notable differences between the characteristics of coupled and decoupled clouds. Coupled ones are generally found in humid environments where vertical atmospheric motions can transport surface fluxes to the cloud base. In contrast, decoupled clouds are typically present in colder and drier environments where vertical motions cannot effectively transport fluxes to the cloud base. These results underscore the complexity of interactions between land and atmosphere and suggest avenues for future research.

1. Introduction

Planetary Boundary Layer (PBL) processes are key players in convection initiation and the formation and evolution of boundary-layer clouds (Berg et al., 2013; Berg & Stull, 2005; Betts, 2009; Golaz et al., 2002; Qian et al., 2013; Teixeira & Hogan, 2002). These low-level clouds are propelled by the earth's surface forcings, such as heat, momentum, and substance fluxes (Betts, 2009; Ek & Holtslag, 2004; Golaz et al., 2002; Jensen et al., 2016; Jensen & Del Genio, 2006; Santanello et al., 2018; Teixeira & Hogan, 2002; Y. Zhang et al., 2017; Zheng et al., 2018b). These fluxes are transported through the PBL to the cloud bases, giving rise to cloud-surface coupled systems (Cheruy et al., 2014; Wu et al., 1998; Zheng & Rosenfeld, 2015). However, not all low-level clouds respond uniformly to these surface forcings. Marine boundary layer clouds, for instance, often rely on cloud-top radiative cooling during weak surface flux conditions, leading to decoupled cloud systems (Bretherton et al., 2007; Moeng et al., 1996; Zheng et al., 2018b). These contrasting interactions between coupled and

Writing – review & editing: Tianning Su, Zhanqing Li, Youtong Zheng, John Yorks

decoupled clouds result in unique differences in their characteristics, development, and evolution, highlighting the important role of cloud-land-surface coupling in the development of cloud systems, especially for low clouds (Hogan et al., 2009; Zheng et al., 2018b).

The interaction between clouds and land surface has long been studied. Previous investigations recognized its importance in the characteristics and evolution of marine clouds (Dong et al., 2015), linking the cloud-surface coupling state to key marine cloud processes, such as the stratocumulus to cumulus transitions (Bretherton & Wyant, 1997; Wyant et al., 1997; Zheng et al., 2018a, 2021; Zheng & Li, 2019) or the probability of Arctic clouds to contain or form ice (Griesche et al., 2021). However, most knowledge about cloud-surface coupling is concerned with cloud-topped marine boundary layers (Albrecht et al., 1995; Bretherton & Wyant, 1997; Dong et al., 2015; Wood, 2012; Zheng et al., 2018a, 2018b; Zheng & Li, 2019). In a marine environment, the definition of a coupled cloud indicates that the moist conserved variables, such as the equivalent potential temperature, are vertically well-mixed through the PBL (Dong et al., 2015). This definition of coupled regime encounters disparities when applied to continental clouds due to differences in PBL definitions and its determination methods between marine and continental environments (Garratt, 1990; Vogelezang & Holtslag, 1996). Consequently, the understanding of cloud-surface coupling over land is still developing, warranting further investigation to fully comprehend these complex interactions.

Following the parcel theory, the lifted condensation level (LCL) and cloud base height (CBH) have been used to determine the coupling state, as their distance dictates it (Dong et al., 2015; Glenn et al., 2020; Zheng et al., 2020; Zheng & Rosenfeld, 2015). In theory, in a coupled state, the LCL should align with the CBH when the potential temperature and the humidity are uniformly distributed in the vertical. However, the CBH and the LCL can differ significantly over land due to the large vertical variability of the thermodynamic variables over continents (Driedonks, 1982; Guo et al., 2016, 2021; Stull, 1988). This discrepancy poses challenges in accurately diagnosing the coupling regime. Su et al. (2022) attempted to tackle this issue by developing a methodology that uses LiDAR data to retrieve the PBL Height (PBLH), combining it with CBH and LCL retrievals to diagnose the coupling regime over the U.S. Southern Great Plains (SGP).

Previous studies on cloud-land interactions have primarily focused on understanding how land surface heterogeneity, evaporative fraction, and soil moisture contribute to the development of shallow convection and its transition to deep convection (Santanello et al., 2018). Some research has linked the strength of land-cloud interactions to the formation and evolution of clouds (Fast et al., 2019; Lee et al., 2019; Xian et al., 2023). However, most of these studies have concentrated on local convection and its role in precipitation, without exploring the differences in cloud-land interactions across various cloud regimes or locations. Recently, Su, Li, Zhang, et al. (2024) examined the role of sensible heat flux in cloud-surface coupling during stratiform and cumulus cloud regimes, finding that coupled stratiform clouds dominate under low sensible heat conditions, while coupled cumulus clouds form during high sensible heat fluxes.

Despite the advancements in the understanding of cloud-surface coupling, existing studies remain geographically constrained, with a predominant focus on the SGP (Su et al., 2022; Tao et al., 2019). Additionally, some analyses concentrate on specific seasons, mainly warm seasons (Fast et al., 2019), and do not evaluate the temporal variability of this process. This limited scope restricts our ability to fully understand the coupling processes between clouds and the land surface and their broader influence on the PBL across diverse climatic, geographical, and temporal settings. Since cloud-surface coupling plays a key role in regulating PBL evolution, stability, and aerosol–cloud interactions (Su, Li, Henao, et al., 2024; Su et al., 2025; Zheng et al., 2021), establishing a more extensive climatological framework is essential. A broader climatology of cloud-surface coupling can provide helpful insights into the variability and evolution of cloud dynamics under diverse conditions. In particular, how differently the percentages of coupled and decoupled clouds manifest across environmental conditions and geographical regions, and what primary processes drive these differences, remain open questions. Furthermore, examining cloud-surface coupling across various regions and temporal scales could clarify how differences and similarities in factors such as vegetation, soil moisture, altitude, and other environmental elements influence cloud dynamics, formation, evolution, cloud regimes, and ultimately precipitation.

To address some of this gap, this study leverages the extensive observational resources provided by the Department of Energy's Atmospheric Radiation Measurement (ARM) User Facility. ARM offers ample and continuous observations of a wide range of atmospheric variables at different fixed sites and field campaigns have been made available to study atmospheric processes including those concerning PBL and cloud variabilities,

Table 1
List of ARM Site Specifics and Mean Meteorological Factors

Site	Latitude	Longitude	Elevation (m.a.s.l.)	Period	Number ASRL cases analyzed	Mean PBLH (m.a.g.l)	Mean SH (W/m^2)	Description
SGP	36°36′ 26.36″ N	97°29′ 15.51″ W	314	04/2001–09/2019	100,564	907	ECOR: 94.5 BAEBBR: 48.7	Midlatitude plain
MAO	3°12′46.7″ S	60°35′ 53.16″ W	50	01/2014–11/2015	7,903	943	74.9	Tropical rain forest
COR	32°4′0.91″ S	64°52′ 53.6″ W	1141	10/2018–04/2019	4,543	584	91.1	Midlatitude mountain
TMP	61°50′ 34.8″ N	24°17′16.8″ E	179	02/2014–09/2014	4,139	748	Not Available	Boreal forest
FKB	48°32′ 24.36″ N	8°23′48.48″ E	511	04/2007–12/2007	5,809	742	26.3	Midlatitude mountain forest

among others (Sisterson et al., 2016; Xie et al., 2010). By leveraging ARM's robust and diverse observational capabilities at five sites with different climatic regimes, this study aims to provide a climatology of cloud-surface coupling in different geographical locations of various meteorological conditions. This investigation aims to enhance our understanding of the interactions between clouds, the PBL, and the land surface, providing insights that may benefit other pertinent studies.

The paper is organized as follows. The second section outlines the data and methodology for assessing cloud-surface coupling following both thermodynamic and remote sensing approaches. The third section presents major research findings, which include the evaluation of coupling thresholds, the climatology of cloud-surface coupling for diurnal and seasonal variations, and the thermodynamic and dynamic perspective of the coupled and decoupled conditions. The paper concludes with a discussion section.

2. Data and Method

2.1. DOE ARM Sites

The ARM User Facility, funded by the U.S. Department of Energy, has been making atmospheric observations since 1992, providing information on clouds and aerosol properties and their impacts on the Earth's energy balance at multiple sites across the globe. The variety of geographical and climatical conditions observed by the ARM and the vast set of sensors at each site makes ARM data suitable for the investigation of cloud-surface coupling.

This investigation used data from five ARM sites, including one permanent site, the SGP, and four mobile facilities. Specifically, the SGP site, located in the central United States, is ARM's oldest and most extensive observatory, providing information on continental cloud formations for more than two decades (Sisterson et al., 2016). The GoAmazon (MAO) campaign investigated the tropical cloud lifecycle and atmospheric composition over the Amazon rainforest from January 2014 to November 2015 (Martin et al., 2016). The CACTI (COR) campaign in the Sierras de Córdoba mountain range in Argentina captured cloud systems over complex terrain from October 2018 to April 2019 (Varble et al., 2021). The BAECC (TMP) campaign deployed in a boreal forest in Hyytiälä, Finland studied the impact of biogenic aerosols on clouds and climate (Petäjä et al., 2016). Finally, the COPS (FKB) campaign in the Black Forest in Germany aimed to improve understanding and forecasting of convective precipitation in complex terrain (Wulfmeyer et al., 2011). Additional information on different sites, including the site's location, elevation, and data record period, are presented in Table 1.

For cloud boundary products, the Active Remote Sensing of Clouds (ARSCL, DOI: 10.5439/1228769) data set was used (Clothiaux et al., 2000). At the SGP site, the CLDTYPE product (CLDTYPE, DOI: 10.5439/1349884), derived from ARSCL, was utilized. For the COR and TMP sites, the raw ARSCL product using the KAZRARSCL—Ka-Band ARM Zenith Radar (KAZR) Active Remote Sensing of Clouds (ARSCL)—algorithm was employed (Kollias et al., 2020). For MAO and FKB, the W-band Cloud Radar Active Remote Sensing of Cloud (WACRARSCL, DOI: 10.5439/1987955) was used. The PBLH was computed using micropulse LiDAR

backscatter profiles, with a vertical resolution of 15 m, averaged to a 10-min resolution, following the methodology described by Su et al. (2020) and Roldán-Henao et al. (2024). At SGP, sensible heat fluxes were obtained from two products: the Energy Balance Bowen Ratio system (EBBR) and the eddy correlation flux measurement system (ECOR).

ECOR employs the eddy covariance technique, which analyzes the correlation between the vertical and horizontal wind components, as well as air temperature, water vapor density, and CO2 density. A primary limitation of this product is the energy budget closure issue, where the combined measured latent heat (LH) and sensible heat (SH) is often less than the measured net radiation minus the soil heat flux (Tang et al., 2019). For instance, Twine et al. (2000) examined the surface budget closure problem using measurements from the Southern Great Plains 1997 Hydrology Experiment and found a systematic closure gap of 10%–30%. To address this, we utilize the ARM value-added product quality-controlled ECOR (30QCECOR, DOI: 10.5439/1097546), which incorporates various corrections. While these adjustments are not specifically designed to ensure energy closure, they do enhance the overall energy budget closure.

EBBR calculates bulk aerodynamic fluxes based on observations of net radiation, soil surface heat flux, and vertical gradients of temperature and relative humidity. In contrast to ECOR, EBBR inherently closes the energy budget. However, this technique does have several limitations that impact its estimations during the periods of strongly stable or unstable atmospheric conditions (Wang & Dickinson, 2012), as well as when the Bowen Ratio approaches −1, typically occurring at sunrise or sunset. To mitigate these issues, we employed the ARM value-added product known as the best-estimate fluxes derived from EBBR measurements and Bulk Aerodynamic calculations (30BAEBBR, DOI: 10.5439/1027268).

ECOR measures chiefly fluxes over winter wheat fields while EBBR measures mostly over grassland at SGP. Therefore, both data sets show systematic differences in measured fluxes caused by the different seasonality of the vegetation growing cycles of wheat and grass (Tang et al., 2019). For MAO, COR, and FKB, only the ECOR data sets are available. No heat fluxes were measured for the TMP site. Temperature and relative humidity profiles were gathered using radiosondes at all five sites. These radiosondes were typically launched at 5, 11, 17, and 23 UTC at each ARM observatory, with SGP having over 1,000 launches and MAO having more than 100 during those times. In the case of COR, launches occurred at different times, primarily during local daytime hours. LCL was computed using ARM meteorological data, including relative humidity, temperature, and atmospheric pressure (MET, DOI: 10.5439/1786358), and following the method outlined by Romps (2017). Finally, vertical velocity data were obtained from the ARM Doppler LiDAR Vertical Velocity Statistics Value-Added Product (sgpdlprofwind4news, DOI: 10.5439/1178582).

It is important to mention that the SGP site stands out with its comprehensive database, spanning over 20 years. Such a large data set yields SGP a statistically robust climatology. Conversely, the remaining sites with data records shorter than 2 years have greater uncertainty in their derived statistics. Additionally, measurements in complex terrains, such as COR and FKB, may be subject to larger sampling errors due to the heterogeneity of boundary-layer clouds over mountainous regions. For example, the ARM sites may be located in areas with preferentially more of fewer clouds. Despite the potential limitations, we include these sites in our analysis as they presently serve as the primary and invaluable source of information for their specific meteorology and environment.

2.2. Identification of Cloud-Land-Surface Coupling

2.2.1. Thermodynamic Definition

Thermodynamic definitions of the state of cloud-surface coupling have been widely applied to marine environments based on moist conserved variables (Bretherton & Wyant, 1997; Dong et al., 2015; Jones et al., 2011; Zheng & Li, 2019). In the case of marine stratocumulus, a coupled situation is usually defined when the liquid water potential temperature varies less than a certain threshold (i.e., 0.5–1 k) below the sub-cloud layer (Jones et al., 2011). In other words, coupled cases are characterized by a well-mixed BL with vertically uniform moist conserved variables. On the contrary, a decoupled state occurs when the moisture conserved variables are vertically stratified (Zheng & Li, 2019).

Following similar criteria used for marine conditions (e.g., Dong et al., 2015; Jones et al., 2011), Su et al. (2022) extended this thermodynamic definition to continental clouds at the SGP site. They defined a coupled state when

the potential temperature (θ) difference between the CBH and the PBLH is less than 1 K (Coupled: $\Delta\theta = \theta_{(\mathrm{CBH})} - \theta_{(\mathrm{PBLH})} < 1\mathrm{K}$). The rationale behind this threshold lies in the role of temperature inversions in limiting the transport of turbulence and heat fluxes between the cloud layer and the land surface. A relatively well-mixed sub-cloud layer indicates efficient mixing, leading to turbulent coupling between the cloud, PBL, and land surface. Potential temperature is not a conserved variable in a moist adiabatic process; however, since the temperature profile is taken inside the sub-cloud layer, this limitation does not affect the identification results.

Using the ARM daytime radiosondes, we employ this thermodynamic approach to compute the coupling state at the five ARM observatories. This approach provides a robust determination of the coupling state. However, since radiosonde measurements are limited in time, additional techniques with higher temporal resolutions are necessary to allow for tracking the diurnal evolution of the coupling regime and conducting a climatological investigation of continental cloud-surface coupling.

2.2.2. PBLH-Based Criteria

PBLH is a key parameter in diagnosing cloud-surface coupling because it represents the top of the turbulent mixing layer where surface influences are transmitted upward. This makes PBLH an effective criterion for assessing whether clouds are dynamically coupled to the surface, as it provides direct evidence of the PBL's vertical extent and its interactions with cloud bases. Following this idea, Su et al. (2022) developed a method to determine the coupling regime of continental clouds using the PBLH from Micropulse LiDAR, the surface meteorology, and the CBH. A coupled cloud is identified if the CBH resides close to or below the previous position of the PBLH, using the LCL as an additional constraint, as per Equation 1:

$$\text{Coupled Cloud: } \mathrm{CBH}(i) < \mathrm{PBLH}(i-1) + A_1 \text{ or } |\mathrm{CBH}(i) - \mathrm{LCL}(i)| < A_2 \quad (1)$$

where i is the time step and A_1 and A_2 correspond to empirical parameters computed based on a sensitivity analysis of the commission and omission errors, in which the thermodynamic approach is taken as the truth. This method depends critically on the estimation of the PBLH. An underestimation of the PBLH leads to an underestimation of coupled cases, and vice versa for the overestimation of coupled cases. This study uses the PBLH output of the DTDS algorithm (Su et al., 2020), which has been shown to outperform traditional LiDAR methods to compute the boundary layer height. DTDS was computed and tested at the same five ARM sites used in this investigation (Roldán-Henao et al., 2024), having higher correlations (as high as 0.93 at the MAO site) and smaller errors than previous LiDAR-based PBLH provided by the ARM.

In this study, we used a similar approach as Su et al. (2022) with minor modifications. First, we removed the LCL constraint and computed the coupling state based only on the difference between CBH and the PBLH as

$$\text{Coupled: } \mathrm{CBH}(i) - \mathrm{PBLH}(i) < A_1 \quad (2)$$

Second, we incorporated an additional step to detect clouds that are adjunctly coupled to the surface. The definition of an adjunct coupled cloud arises from the idea that strong updrafts can rapidly lift convective clouds beyond the PBLH. In such cases, a coupling assessment based solely on Equation 1 could lead to a decoupled classification, even when the cloud's properties still reflect a coupled state. This approach considers the horizontal and vertical extension of clouds, recognizing that coupling does not occur at a single point but over a cloud entity. This is exemplified by updrafts and downdrafts occurring simultaneously in different parts of a cloud. Therefore, our analysis addressed this problem by incorporating the cloud-top height (CTH). If a cloud is initially classified as decoupled, we then check whether it was coupled in the preceding time step. If yes, it is subject to a further test to determine whether the current CBH is below the previous CTH. If so, its coupling state is changed from decoupled to coupled. This additional step of identifying coupling considers the dynamic nature of cloud development and movement and accounts for the transient nature of atmospheric processes. One potential caveat to this methodology is that, in some cases, the side of a tilted cloud moving over the sensors may be mistakenly identified as the cloud base.

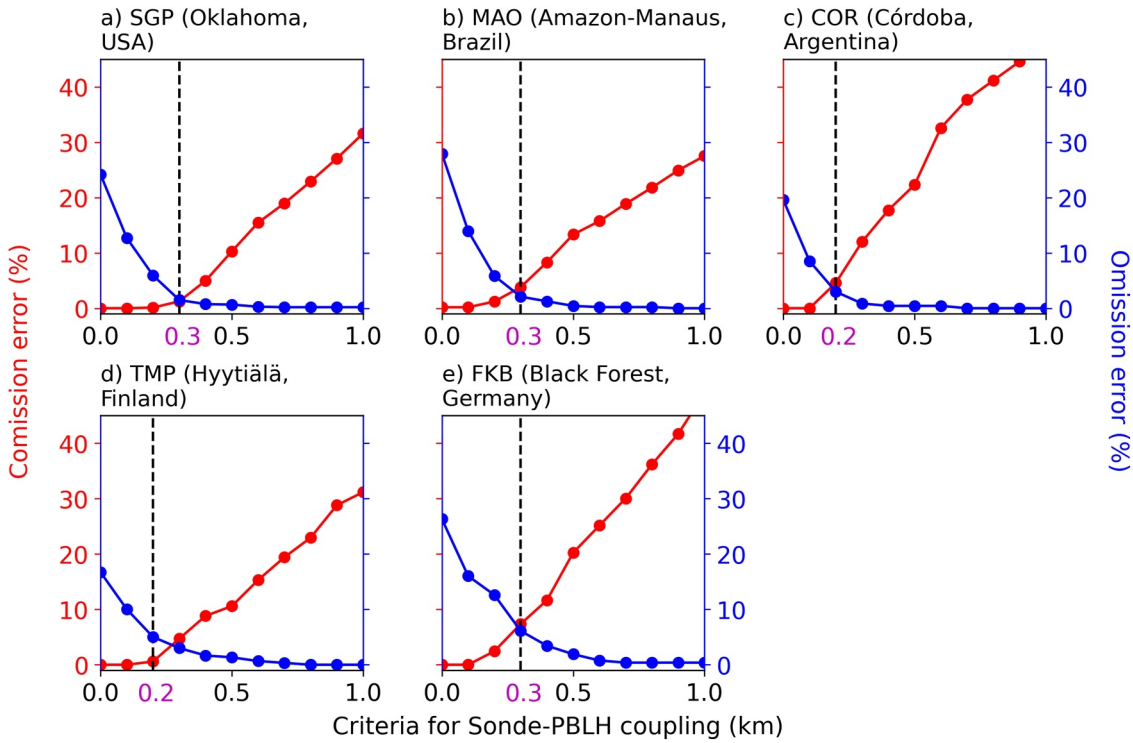

Figure 1. The commission and omission errors as a function of the coupling thresholds used at the five ARM sites. The dashed line indicates where the commission and omission errors are crossover of the same magnitude. The number in magenta is the coupling threshold.

2.3. Establishing Cloud-Surface Coupling Thresholds at ARM Sites

As highlighted in Section 2.2, the cloud-surface coupling depends on an empirical coupling threshold, A_1, determined by conducting a sensitivity analysis on commission and omission errors, with the thermodynamic approach serving as the reference value. The commission error, or "false positive" represents the percentage of decoupled clouds erroneously classified as coupled clouds. Conversely, the omission error, or "false negative," represents the percentage of coupled clouds misidentified as decoupled. Radiosonde estimates of the PBLH being considered as the ground truth, were used to calculate the coupling thresholds. This avoids introducing errors resulting from LiDAR uncertainties and limitations. Both the thermodynamic and PBLH coupling approaches were evaluated based on radiosonde information to establish the coupling thresholds. These thresholds were then applied to evaluate cloud-surface coupling using LiDAR PBLH estimations following Equation 2.

The sensitivity analysis results are presented in Figure 1, which shows the commission and omission errors for different coupling thresholds. The optimal threshold is identified at the intersection point of the two error curves. This interception point minimizes both errors simultaneously, but it does not necessarily minimize the total error. Surprisingly, its value oscillates within a narrow range between 0.2 and 0.3 km across different locations. This consistency suggests the robustness of the method and hints that similar mechanisms may govern cloud-surface coupling across diverse regions. However, due to the limited number of sites, future studies should explore this possibility over broader areas and through theoretical frameworks or model simulations. Further discussion on these mechanisms will be presented in the subsequent section, shedding light on the mechanisms of coupling processes between cloud and land surface. In sum, this approach ensures that the established thresholds are scientifically sound and applicable across various ARM sites, lending confidence in the reliability of cloud-surface coupling determination.

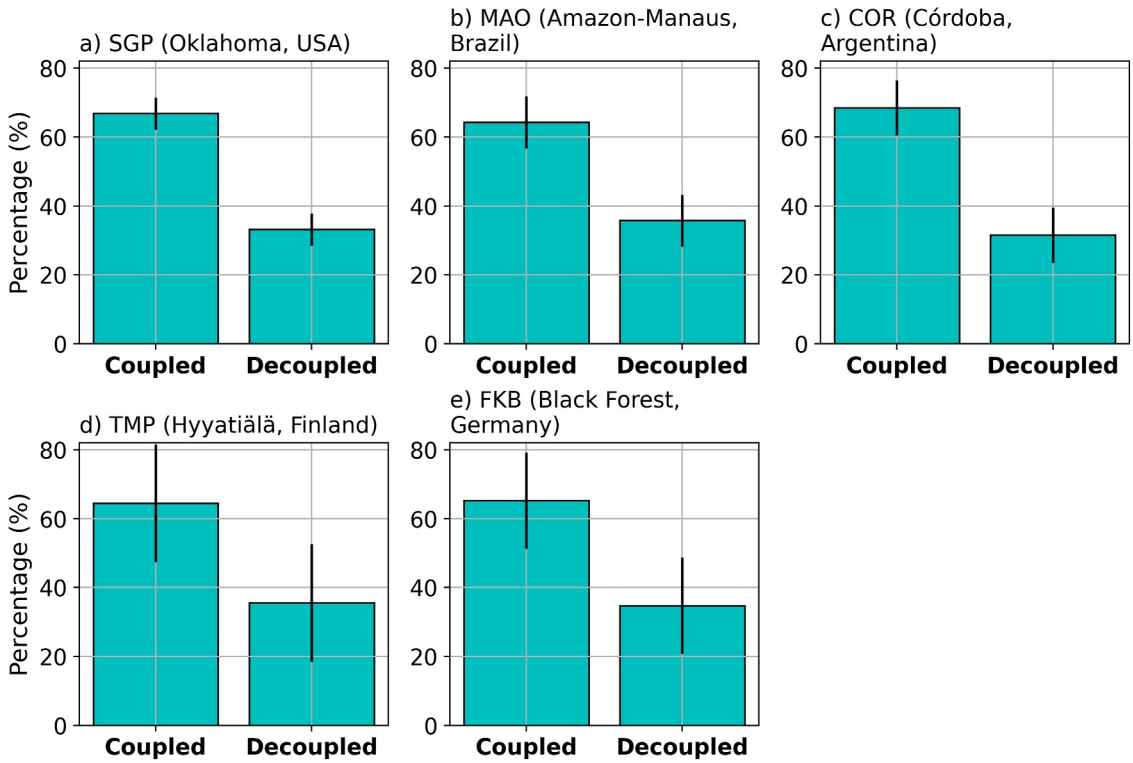

Figure 2. Average percentages of coupled and decoupled low-level clouds at the five ARM sites. Each bar represents the mean percentage with an error bar indicating the standard deviation. Coupled conditions have the following means (±SD): SGP 66.81 ± 4.65%, MAO 64.98 ± 7.54%, COR 68.44 ± 7.99%, TMP 64.44 ± 17.08%, and FKB 65.23 ± 13.94%. Decoupled conditions show corresponding means of 33.18 ± 4.64%, 35.73 ± 7.54%, 31.55 ± 7.99%, 35.55 ± 17.08%, and 34.77 ± 13.94%.

3. Results and Discussion

3.1. Climatological Patterns of Cloud-Surface Coupling Across ARM Sites

Figure 2 illustrates the average percentage of coupled and decoupled clouds at the five ARM sites. These percentages are relatively similar independent of the geographical location, with approximately 65.84% ± 10.24% of the low-level clouds classified as coupled and 34.16% ± 10.24% as decoupled. An explanation for this consistency may lie in a similar role that surface fluxes and PBL dynamics could play in driving cloud formation and evolution, though this interpretation is limited by the spatial and temporal extent of the current data set employed. Surface fluxes of heat, moisture, and momentum are critical in maintaining the turbulence necessary for cloud formation. When these fluxes are strong enough to reach the cloud base, they facilitate the coupling of clouds with the surface. This mechanism could operate in a comparable manner across various climatic regions, as suggested by the consistent coupling percentages.

The similarities in the coupling percentages are evident not only in the average values but also extend to the diurnal variability of the two cloud regimes. Figure 3 shows the diurnal variability of coupled and decoupled percentages at the five ARM observatories. A common feature emerges independent of the geographical location: the percentage of coupled clouds increases in the morning and declines later in the afternoon. Despite the similar general trend, each site experiences the maximum percentage of coupled clouds at different times. For instance, the SGP site peaks around 2:00 p.m., while MAO peaks between around 11:00 a.m. Interestingly, during the period between 10:00 and 15:00 local time, when most sites experience elevated coupling the separation between coupled and decoupled percentages becomes particularly robust, with non-overlapping standard deviations indicating statistically distinguishable regimes.

The differences in the diurnal variability of coupling percentage can be attributed to local climatic conditions and geographical features that influence the timing and intensity of surface fluxes and PBL development. For the tropical region, such as MAO, the relatively early peak in coupled clouds may be driven by strong latent heat and weak stratification (Tian et al., 2022), which rapidly destabilizes the PBL, promoting convection and cloud

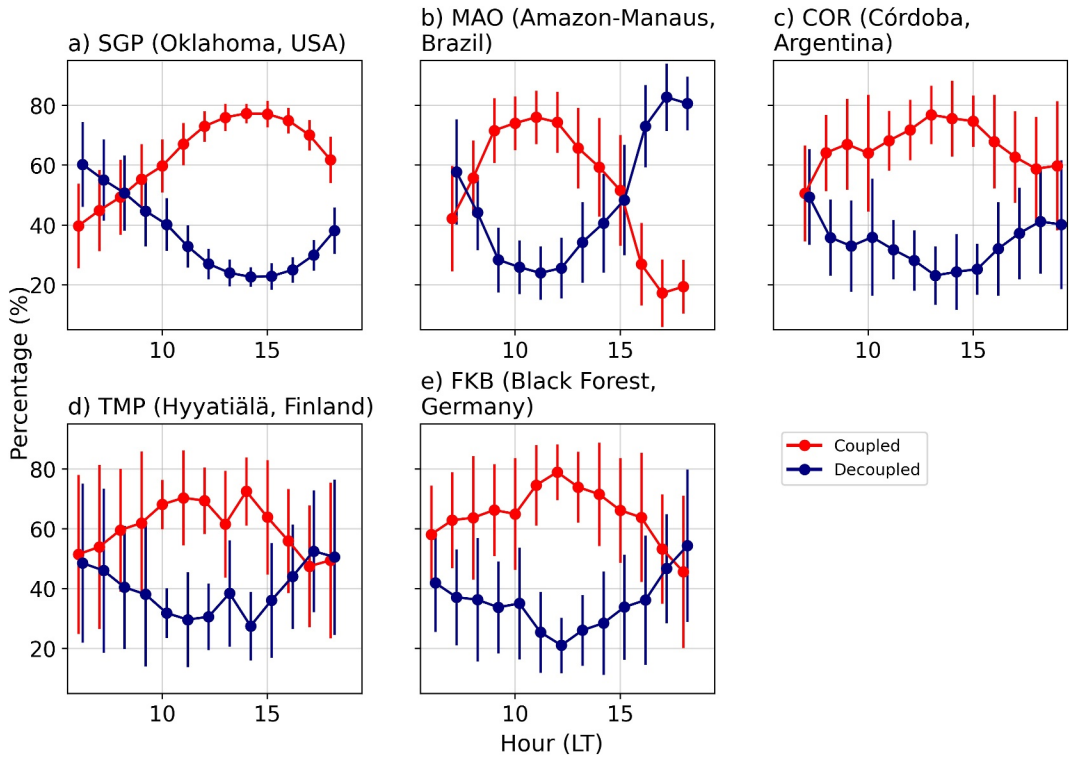

Figure 3. Hourly variation of the percentage of coupled and decoupled clouds at the five ARM observatories. The red lines correspond to the coupled cases while the blue lines represent the decoupled cases. Error bars represent the standard deviation.

formation. The Amazon region's abundant moisture and heat promote the development of strong deep convective systems. However, the precipitation and albedo effects of these cloud systems stabilize the atmosphere and suppress the PBLH, leading to a faster afternoon decline in the percentages of coupled clouds at MAO compared with other sites. Conversely, SGP typically experiences a delayed peak in coupled clouds due to a different set of climatic conditions. The SGP region, characterized by extensive agricultural land, has a slower buildup of surface heat compared with the Amazon and a relatively late development of PBLH compared with other sites (S. Liu & Liang, 2010; Roldán-Henao et al., 2024).

Both COR and FKB are mountainous regions where orographic uplifting and intense deep convection are prominent. The elevation and surface roughness at these sites may generate strong turbulence and convective instability, favoring the formation of orographic boundary-layer clouds. At COR, heat and moisture are frequently transported from the Amazon region by the South American Low-Level Jet (SAMLLJ). Additionally, air often converges east of the COR site in areas with the highest terrain, creating ideal conditions for the formation of boundary-layer clouds coupled with the PBLH. This interaction, combined with COR's subtropical location, influences the diurnal variability of these coupled clouds. In contrast, the forested environment at FKB and TMP provide additional moisture, and the combination of this moisture with limited heat flux, likely supports the formation of coupled stratocumulus layers.

H. Zhang et al. (2024) used large-eddy simulations (LES) within the LASSO framework to examine cloud-surface coupling under shallow convection at SGP. They found a relatively similar diurnal variability for coupled and decoupling conditions, with coupled clouds being lower in the morning and increasing in the afternoon, primarily driven by surface sensible heat fluxes influencing PBLH development. However, LES tended to overestimate afternoon coupling, cloud liquid water path, and cloud-top height—biases attributed to overly rapid boundary layer growth and misrepresentation of shallow convection triggers. Future studies using LES capable of resolving shallow clouds could help clarify the physical mechanisms behind the consistent coupling percentages observed in our analysis.

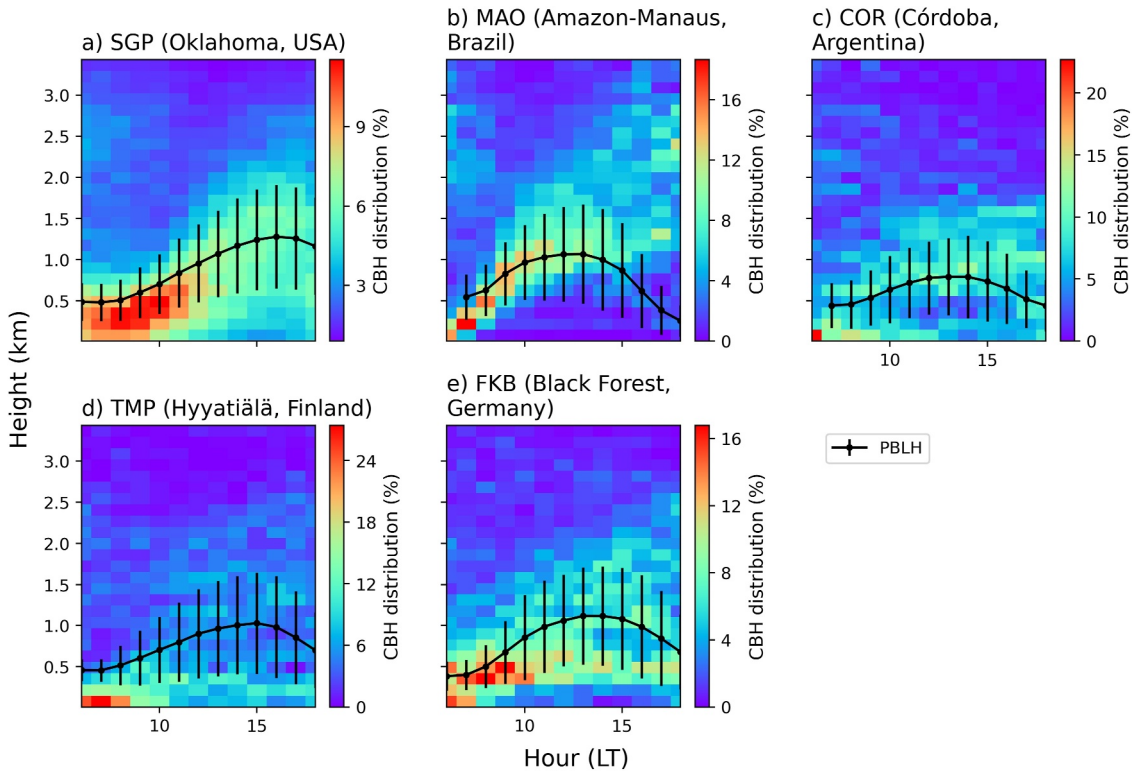

Figure 4. The color background represents the hourly vertical distribution of cloud base height (CBH) at each ARM. The solid black line corresponds to diurnal variation of the planetary boundary layer height and error bars represent the standard deviation.

3.2. Site-Specific Differences in Cloud Coupling and Their Influencing Factors

The observed diurnal variability in Figure 3 is driven by changes in the number of coupled clouds rather than changes in the number of decoupled clouds. As illustrated in Figure S1 in Supporting Information S1, the number of coupled clouds varies along the day, whereas decoupled clouds stay relatively constant. This difference in diurnal variability between coupled and decoupled clouds is expected, given their nature. Coupled clouds directly respond to surface forcings such as heat, moisture, and momentum, which have a strong diurnal cycle, especially for coupled cumulus clouds. Conversely, decoupled clouds, being disconnected from the surface, do not respond to the same forcings, resulting in their less marked diurnal variability. Moreover, the pronounced increase in the number of coupled clouds compared with the stable behavior of decoupled clouds suggests that factors beyond PBLH growth are the drivers of this trend. Specifically, it is likely that coupled clouds also form locally during the day, as previously proposed by Berg and Kassianov (2008) for the SGP site.

Changes in the diurnal variability of the PBLH and the CBH are key to understanding cloud-surface coupling. Figure 4 displays the average diurnal variation of the PBLH at each site (black line) and the vertical distribution of CBH for each hour (heat map). Notably, all five ARM observatories display similar patterns, starting with a shallow boundary layer that deepens throughout the day. As the PBLH increases, more low-level clouds interact with surface forcings, leading to more coupled clouds. As convective conditions strengthen, boundary layer clouds often exceed the PBLH and decouple from the surface as convective thermals weaken and the PBLH declines. At the MAO site, where deep convection is pronounced, this decoupling occurs earlier, with less than 10% of clouds remaining within the mean boundary layer by 1:00 p.m.

Figure 5 compares the diurnal variability of PBLH under coupled and decoupled conditions at each site. Among these, MAO stands out with a noticeably higher PBLH during coupled conditions, likely influenced by stronger sensible heat fluxes. A similar trend appears at SGP, where the mean PBLH is also higher when clouds are coupled. However, the overlapping standard deviation bars between coupled and decoupled conditions suggest that these differences may not be statistically significant.

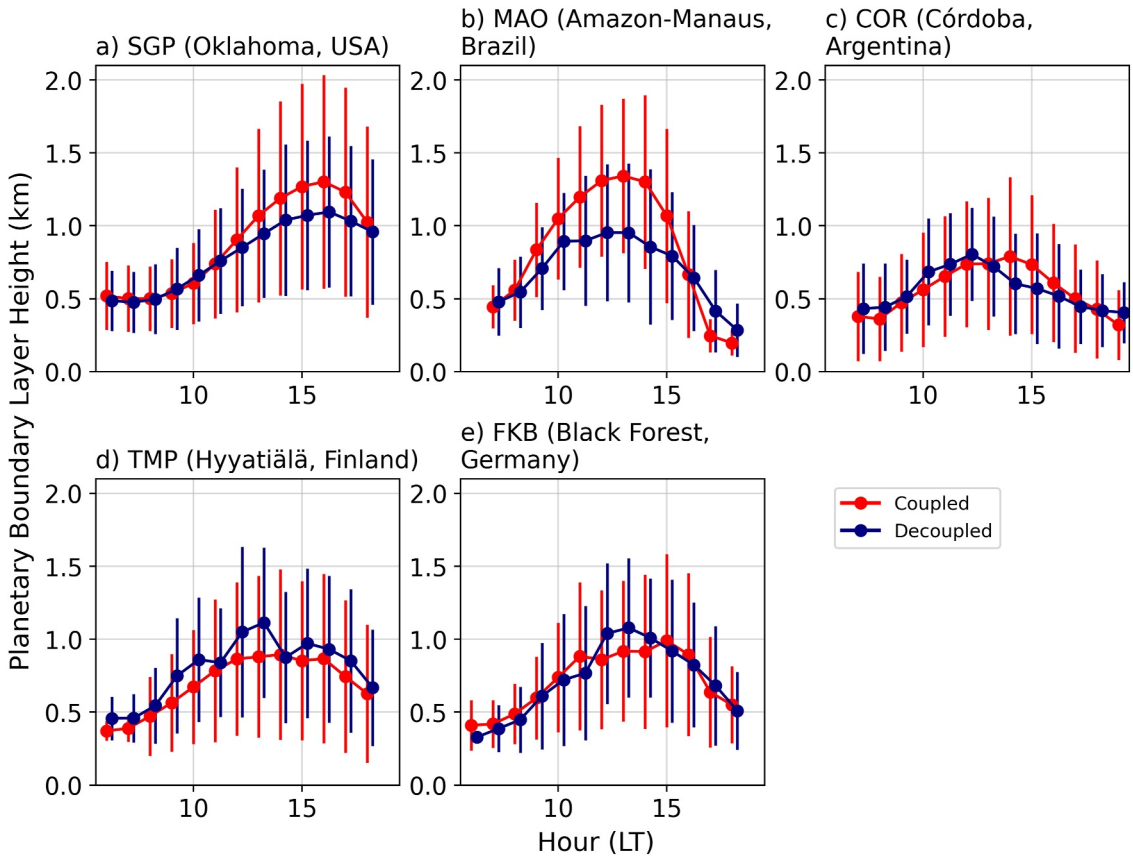

Figure 5. Hourly variation of the Planetary Boundary Layer Height (PBLH) for coupled and decoupled regimes at the five ARM observatories. The red lines correspond to the coupled cases while the blue lines represent the decoupled cases. Error bars represent the standard deviation.

Interestingly, when clouds are further classified into cumulus and stratiform types, more noticeable distinctions in PBLH emerge. At the SGP site (Figure S2a in Supporting Information S1), coupled cumulus clouds tend to occur with deeper boundary layers while coupled stratiform clouds are associated with shallower PBLH. This indicates that a higher PBLH can facilitate coupling by enhancing turbulence and promoting vertical mixing that links the cloud to the surface. Nevertheless, PBLH alone does not determine cloud coupling. Coupled clouds can form under both deep and shallow boundary layers, depending on cloud type and other environmental factors.

While differences in PBLH primarily emerge when cloud types are distinguished, Figure 5 may offer indirect clues about the diurnal distribution of cloud types during coupled conditions. For instance, sites such as MAO and SGP exhibit slightly higher boundary layers during the late morning and afternoon hours, suggesting an increase in the presence of coupled cumulus clouds during those periods, consistent with observations from Figure S2b in Supporting Information S1 at SGP. In contrast, sites such as TMP, where coupled clouds are associated with shallower PBLH compared with decoupled clouds, likely reflect a stronger contribution from coupled stratiform clouds, which aligns with the boreal characteristics of TMP.

In the case of COR, the PBLH under coupled and decoupled conditions differs between morning and afternoon hours, being slightly taller for decoupled clouds in the morning, and slightly taller for coupled clouds in the afternoon. This pattern is weakly reflected in the sensible heat flux (Figure 6), which shows moderately higher values for decoupled clouds in the morning and for coupled clouds in the afternoon. Such a shift may be associated with the influence of coupled stratiform clouds in the morning and coupled cumulus clouds in the afternoon. At FKB, differences are only noticeable between 1:00 p.m. and 3:00 p.m., with higher PBLH values for decoupled clouds. Changes in the CBH for coupled and decoupled clouds are included in Figure S3 in Supporting Information S1. Essentially, decoupled clouds have taller bases than coupled clouds and are located on average between 1.5 and 2.5 km a.g.l.

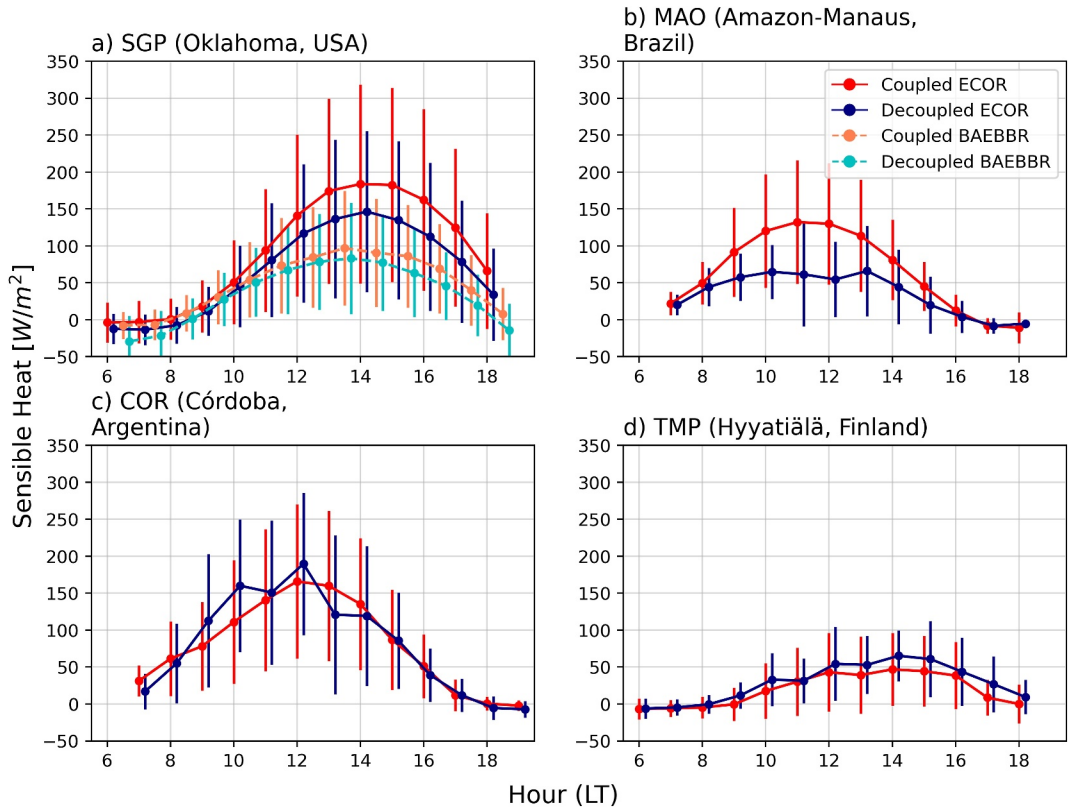

Figure 6. Hourly variation of the sensible heat flux for coupled and decoupled regimes at the five ARM observatories. The red lines correspond to the coupled cases while the blue lines represent the decoupled cases. Solid lines correspond to sensible heat flux taken from the ECOR ARM value-added product while the dash lines correspond to the BAEBBR ARM value-added product.

According to Su, Li, Zhang, et al. (2024), coupled stratiform clouds tend to dominate under low sensible heat flux conditions while coupled cumulus clouds are more prevalent under high sensible heat flux. Figure 6 displays the difference in the sensible heat flux for coupled and decoupled conditions. As expected, differences in the MAO site are the most significant, followed by SGP, with coupled clouds having higher sensible heat flux in the afternoon than decoupled ones, probably associated with increased cumulus coupled clouds. At COR, sensible heat flux is slightly higher for decoupled clouds in the morning and slightly higher for coupled clouds in the afternoon. Therefore, the increase in the number of cumulus coupled clouds at COR may occur much later in the afternoon (probably after noon) than at SGP or MAO. However, given the broad spread of error bars, further investigation that incorporate the different cloud regimes is needed to confirm this interpretation.

3.3. Seasonal Variations in Cloud-Surface Coupling at the SGP Site

The SGP site provides a data record spanning over 20 years, making it the sole site capable of offering a deep insight into seasonal variations in cloud-surface coupling regimes. Figure 7 presents the number of observations for both coupled and decoupled cases across different seasons, along with their respective percentages at SGP. Notably, cloud observations are most frequent in spring. During this season, the Great Plains Low-Level Jet (GPLLJ) transports substantial moisture from the Gulf of Mexico while simultaneously enhancing surface heat fluxes (G. Liu et al., 2013; Song et al., 2019). Additionally, during spring, the SGP site is often located ahead of an upper-level trough, which promotes low-level convergence and upward motion (Song et al., 2019). These atmospheric conditions collectively contribute to increased cloud formation, leading to the higher number of observed clouds during this season.

Despite the increased number of observed clouds in spring, the percentages of coupled and decoupled clouds do not drastically vary among seasons (Figure 7b). Overall, warm seasons have moderately higher coupled

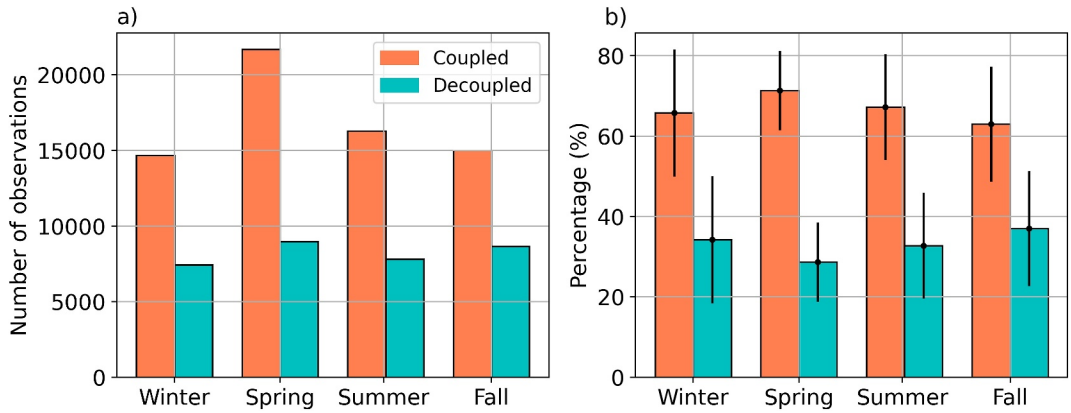

Figure 7. (a) Number of cloud samples for coupled and decoupled conditions among the four seasons at the SGP. This value is the count of cloudy samples in intervals of 10 min and does not represent the actual number of individual clouds. (b) Percentage of coupled and decoupled low-level clouds for each season at the SGP site. Coupled conditions have the following means (±SD): Winter 66.44 ± 15.49%, Spring 72.25 ± 9.6%, Summer 67.84 ± 13.15%, and Fall 63.77 ± 14.1%. Decoupled conditions show corresponding means of 32.56 ± 15.49%, 27.75 ± 9.6%, 32.16 ± 13.15%, and 36.22 ± 14.1%.

percentages, with spring having the maximum percentage with 72.2% ± 9.6% being coupled and fall having the lesser percentage of coupled clouds with 63.8% ± 14.1%. This moderate peak in the number of coupled clouds during warm seasons likely occurs due to a favorable convective environment that promotes boundary layer cumulus cloud formation.

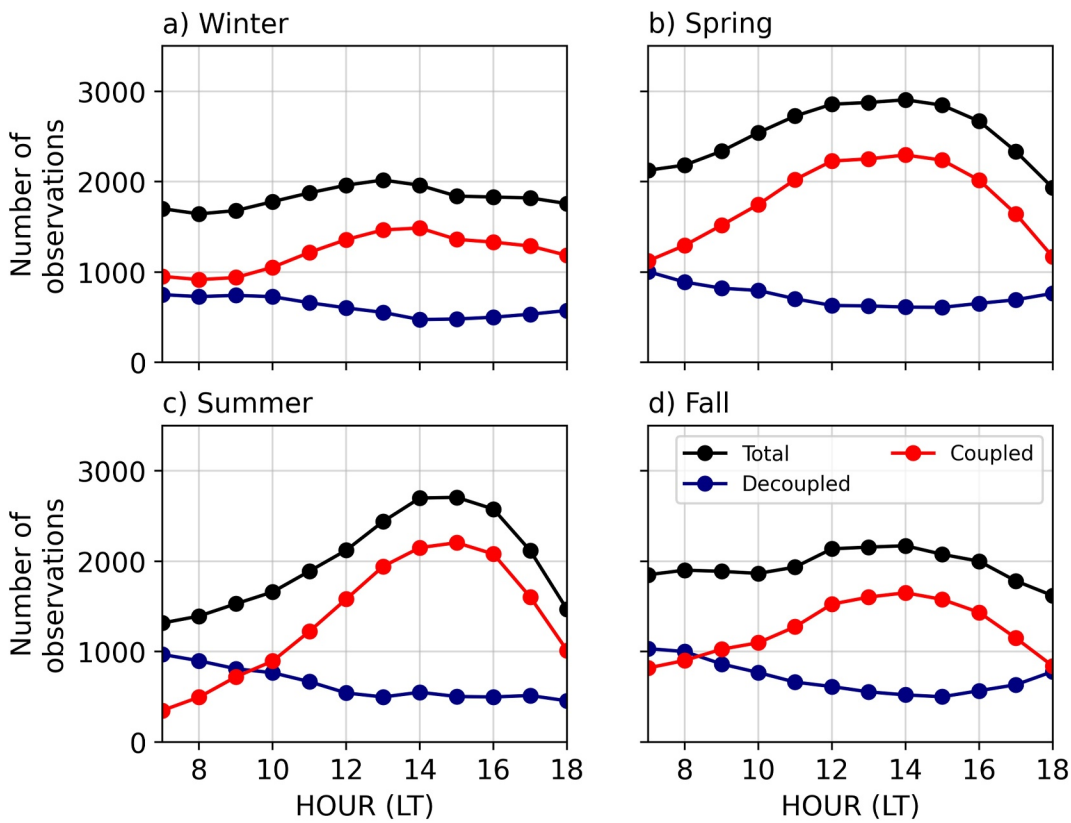

Figure 8. Diurnal variability of the number of observations for coupled and decoupled clouds during (a) winter, (b) spring, (c) summer, and (d) fall at the SGP site.

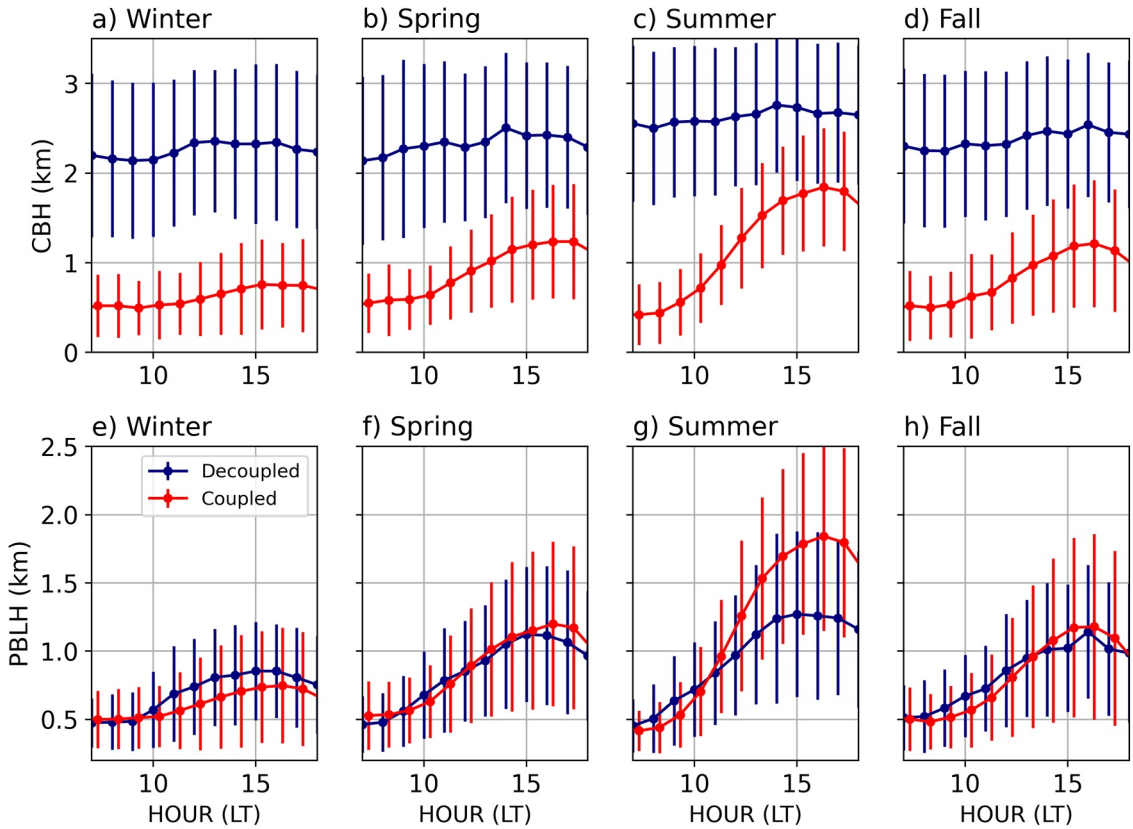

Figure 9. (a) Diurnal variation of the Cloud Base Height (CBH) for coupled (dashed lines) and decoupled (solid lines) conditions across the four seasons. (b) Diurnal variation of the Planetary Boundary Layer Height (PBLH) for coupled (dashed lines) and decoupled (solid lines) conditions across the four seasons.

Figure 8 shows the diurnal variability in the number of coupled and decoupled clouds observed in the four seasons. As shown, the diurnal cycle of coupled clouds is most pronounced during the warmer seasons, with a peak occurring in the afternoon. In spring and summer, surface conditions play a key role in promoting coupling. The combination of warmer temperatures, higher moisture, and strong afternoon surface heating enhances convective mixing from the ground up. In particular, increased sensible heat flux drives the growth of the boundary layer, allowing it to reach cloud base and support the formation of coupled cumulus clouds.

In contrast, in colder seasons, especially in winter, diurnal variation is weak in coupled and decoupled clouds. During this season, colder temperatures and weak surface heat flux typically lead to a shallow PBLH. However, these low temperatures also increase relative humidity, creating favorable conditions for stratiform cloud formation. These clouds can connect with the surface through a top-down convective process, where radiative cooling at the cloud top destabilizes the layer beneath, promoting mixing and establishing a link with the surface. This mechanism may be common in winter, likely contributing to the high percentage of coupled clouds during the season.

Figure 9 shows the hourly variation of the CBH and PBLH for coupled and decoupled clouds across the four seasons. As depicted, the CBHs of decoupled clouds (blue lines) are, on average, above 2 km and do not vary significantly diurnally or seasonally, having shallow bases during winter. In contrast, the CBH of coupled clouds varies significantly both seasonally and diurnally, reaching its highest values during the afternoon hours in summer. This pattern indicates that coupled clouds are more responsive to diurnal heating cycles, where increased solar radiation during the day promotes deeper PBL development and subsequently higher CBH values. These variations reinforce the importance of surface heating in driving the formation and development of coupled clouds.

Regarding the PBLH, coupled conditions (red lines) show higher PBLH values for summer and slightly higher values for decoupled clouds in winter (Figure 10e). In summer, the PBLH under coupled regimes is

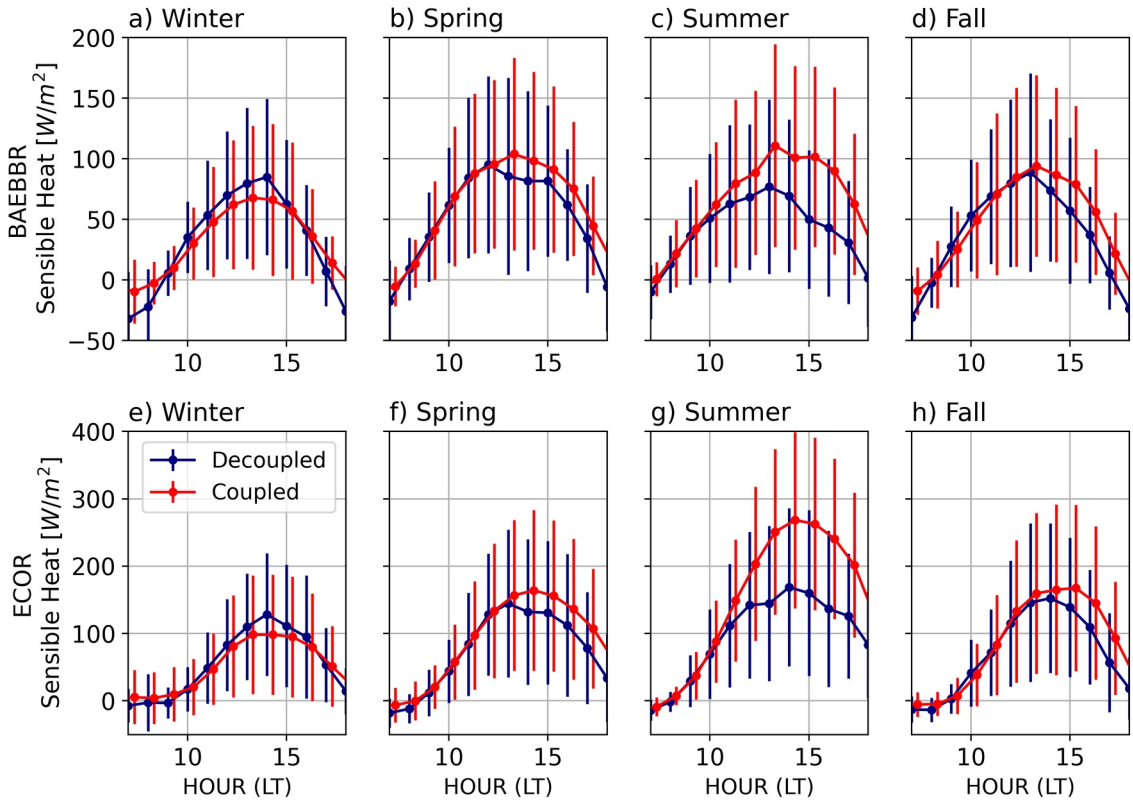

Figure 10. Diurnal variability of Sensible Heat Flux for coupled (dashed lines) and decoupled (solid lines) conditions across the four seasons, (a) based on the ECOR data set and (b) based on the EBBR data set. (C) and (D) stand for Coupled and Decoupled, respectively.

approximately 50% higher than under decoupled regimes. The variations across different seasons could be closely linked with the prevailing cloud regimes during these periods. During the warm season, cumulus coupling is predominant, with high PBLH and strong updrafts serving as the driving forces for forming coupled clouds, resulting in significantly higher PBLH values. Conversely, in winter, stratiform clouds dominate, favoring low PBLH and high humidity conditions with a more neutral PBL structure. In addition, during colder seasons, such as winter, synoptic-scale weather systems become more frequent, leading to the presence of clouds that are unlikely to be coupled to the surface.

Similar to Figures 9 and 10, the diurnal variations of sensible heat flux in both coupled and decoupled situations across the four seasons are illustrated. Figures 10a–10d are derived from the ECOR data set while Figures 10e–10h are based on the EBBR data set. Despite variations in magnitude across data sets and the wide spread standard deviation, both data sets reach the same conclusion: sensible heat fluxes are relatively greater in coupled situations, except during the winter months. Furthermore, the magnitude of the difference between coupled and decoupled regimes is more pronounced during the summer, aligning with prior analyses of the PBLH.

3.4. Dynamic Evidence for the Cloud-Surface Coupling

Vertical movement is pivotal in boundary layer dynamics, intricately linked to the turbulent transport of quantities such as moisture, heat, momentum, and substances (Stull, 1988). To fully understand cloud-surface coupling, a comprehensive grasp of the process's dynamic and thermodynamic aspects is necessary. In this study, we analyzed vertical motions, utilizing the comprehensive data from Doppler LiDAR observations over the SGP central facility site, collected between October 2010 and July 2023.

Figure 11 shows typical examples of a coupled regime (top row) and a decoupled regime (bottom row) observed at the SGP. The left side displays the normalized backscatter signal from the Micropulse LiDAR and the PBLH computed with DTDS and radiosondes. On the right side, the vertical wind speed from the Doppler LiDAR is shown. Figure 11a depicts the coupled case example, where a well-defined boundary layer capped with boundary

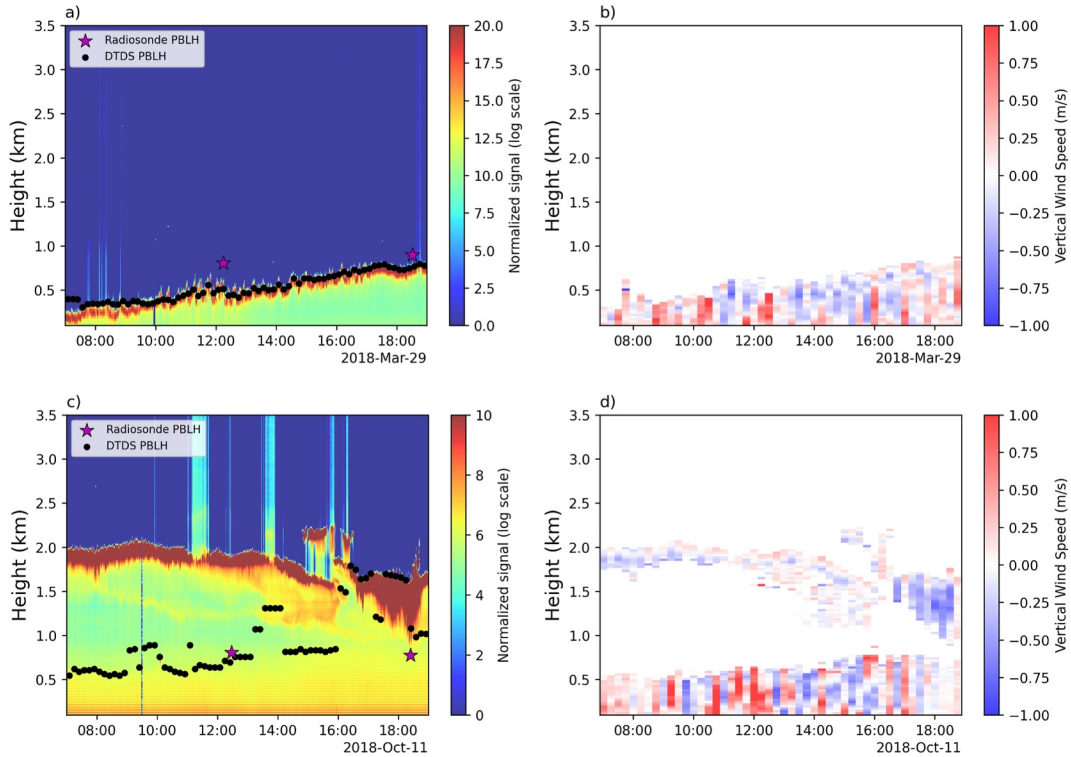

Figure 11. Examples of coupled (a–b) and decoupled (c–d) cloud regimes observed at the Southern Great Plains. (a) Normalized backscatter signal from the Micropulse LiDAR during the coupled regime, the black dots represent the estimated Planetary Boundary Layer Height (PBLH) from the DTDS, and the stars are the radiosonde-based PBLH. (b) Vertical velocity from the Doppler LiDAR for the coupled regime. (c–d) are the same as (a–b) but for decoupled conditions.

layer clouds is observed. During this day, the vertical motions (Figure 11b) consist of upward and downward movements reflecting a boundary layer mixed throughout the day. Of particular interest is that on this day, the vertical motions extend from the surface to the cloud base, connecting the surface directly to the cloud system.

Figures 11c and 11d depict the decoupled case, where the observed clouds are positioned 1 km or more above the PBLH. In this case, we see a similar pattern of upward and downward motions inside the PBL. However, these vertical motions do not extend to the cloud base, creating a clear separation between the top of the PBL and the cloud base. At the cloud base, we can see vertical motions again, associated with turbulence inside the cloud. This detachment between the cloud and the surface prevents surface properties from reaching the cloud system, which is a key difference between both cloud regimes.

In contrast to Figures 11 and 12 presents the diurnal variation of vertical velocity variance averaged over all cloudy data during coupled and decoupled regimes. The figure also includes the PBLH, CBH, and CTH. Under coupled conditions, the CBH closely follows the PBLH, making them indistinguishable in the figure. Coupled conditions exhibit a shallow PBL with weak vertical motions in the morning. As the day progresses, stronger sensible heat fluxes drive a deeper PBLH compared with decoupled cases, enhancing vertical motion from the surface to the CBH. This connection facilitates the transfer of surface properties to the cloud system. For coupled conditions, the PBLH, CBH, CTH, and vertical velocity variance follow similar diurnal cycles, starting with lower values in the morning and intensifying toward peaks in the afternoon.

In decoupled conditions, the PBL also begins as a shallow layer in the morning. However, as the day progresses, its growth remains more limited compared with coupled cases. There is a pronounced gap between the PBLH and CBH, as well as between the vertical motions within the PBLH and those below the cloud layer. This separation is evident in the heatmap in Figure 9b, which shows a region between 1 and 2 km with near-zero vertical velocity variance. Due to the lack of vertical motion above the PBLH, surface fluxes cannot reach the cloud base. As a

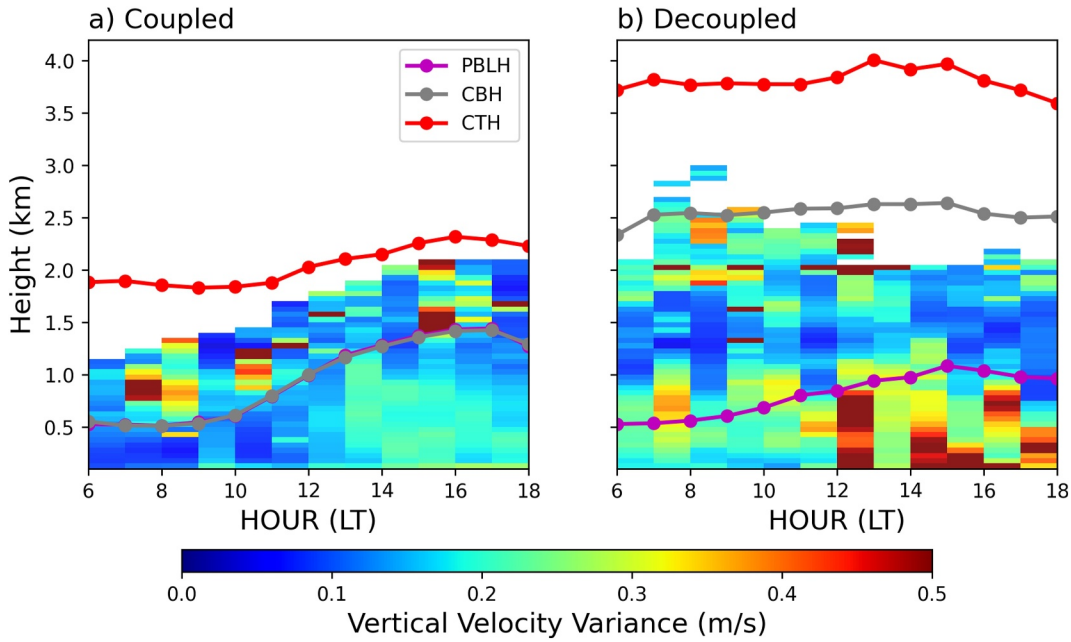

Figure 12. Diurnal variability of the vertical velocity variance at different heights measured at the Southern Great Plains for (a) coupled and (b) decoupled situations. The purple line corresponds to the Planetary Boundary Layer Height (PBLH), the gray line is the Cloud Base Height (CBH), and the red line is the Cloud Top Height (CTH). Notice that in (a) the PBLH is not visible since it is almost identical to the CBH.

result, decoupled clouds exhibit minimal diurnal variability, with both CBH and CTH remaining nearly constant throughout the day.

3.5. Relationship Between Cloud-Surface Coupling and Thermodynamic Profiles

A comprehensive understanding of the climatology of cloud-surface coupling requires examining both its dynamic and thermodynamic aspects. Figure 13 presents the vertical profiles of equivalent potential temperature and relative humidity for coupled and decoupled cloud conditions at the SGP site, distinguishing between morning and afternoon soundings.

For coupled conditions, surface temperatures are lower in the morning than in the afternoon, leading to a lower LCL and higher near-surface relative humidity (see Figure 13). These thermodynamic characteristics are consistent with the stratiform coupling regime, which dominates under low sensible heat conditions (Su, Li, Zhang, et al., 2024). The combination of a shallow PBL and high near-surface humidity in the morning supports the persistence of stratiform clouds that remain coupled to the surface. In the afternoon, increased surface heating deepens the PBL, enhancing turbulent mixing and reducing near-surface humidity. This transition is accompanied by increased buoyancy and lower humidity at cloud base, as revealed by the temperature and humidity profiles in Figure 13, favoring a shift to cumulus coupling, where cloud formation is driven by localized convection.

In contrast, decoupled clouds exhibit distinct thermodynamic features. Surface temperatures remain relatively unchanged throughout the day, and their relative humidity profile peaks at higher altitudes (2–4 km). These clouds also feature a drier lower atmosphere than the coupled counterparts. In such a colder and drier lower atmosphere with a low PBLH (see Figure 5a), the formation of boundary layer clouds is difficult, suggesting that the decoupled clouds could be linked to large-scale forcing, such as advection, or be the remaining cloud of a strong convective system after convective thermals cease and the boundary layer decays. Other factors can also result in decoupling by increasing stratification within the boundary layer. For example, precipitation can suppress vertical mixing by warming the cloud layer (via latent heat release) and cooling the subcloud layer through evaporation, which leads to a stable layer between the boundary layer and the cloud base. Daytime insolation can drive diurnal decoupling by warming the cloud layer more than the subcloud layer (Nicholls, 1984; Turton and Nicholls, 1987). In the case of stratiform clouds and during weak capping temperature inversion, the warming from entrainment

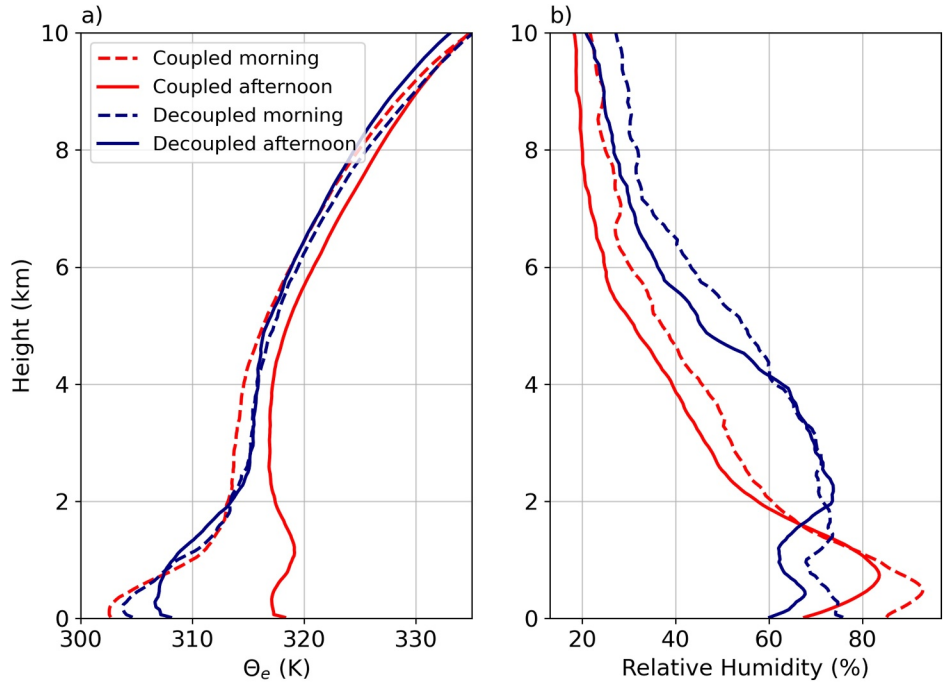

Figure 13. (a) Average equivalent potential temperature (θ_e) for coupled (red) and decoupled (blue) situations. The dashed lines correspond to the morning radiosondes launched at 6:00 a.m. at the SGP site; the solid line corresponds to the afternoon radiosondes launched at noon. (b) Same as (a) but for relative humidity.

can offset the cloud-top radiative cooling, reducing buoyancy production and leading to a less convective, more stratified boundary layer, thus promoting decoupling (Bretherton & Wyant, 1997; Zheng et al., 2021).

4. Summary and Discussion

This study presents a comprehensive climatology of cloud-land-surface coupling across various Atmospheric Radiation Measurement (ARM) sites, offering insights into the dynamic and thermodynamic conditions influencing clouds and their interaction with terrestrial processes. Through the analysis of long-term observational data, we refine our previously proposed method of determining the state of coupling with new thresholds, evaluate direct and adjunct coupling mechanisms, and explore the climatological patterns of coupled and decoupled cloud conditions. Our method encompasses an examination of sensible heat fluxes, thermodynamic profiles, and Doppler LiDAR measurements to distinguish between coupled and decoupled cloud states, thereby elucidating the influence of surface fluxes on cloud dynamics.

Consistent coupling thresholds are revealed across the five ARM sites, and the fractions of coupled and decoupled clouds out of low-level clouds are also rather invariant, averaging 65.84% ± 10.24% and 34.16% ± 10.24% respectively. Our analysis further highlights distinct thermodynamic and dynamic characteristics between the two regimes. Coupled cumulus clouds can occur under either deep or shallow PBLH conditions and during periods of strong or weak surface fluxes; these variations are attributed to differences in cloud type. While a high PBLH facilitates cloud-surface coupling, it is not a determining factor. Dynamically, coupled clouds are sustained by turbulent vertical motions that connect them to the surface.

In contrast, decoupled clouds exhibit a weak connection to surface forcing, and accordingly, no significant diurnal variations are observed. Decoupled conditions are typically favored under weak surface fluxes and drier environmental conditions. These clouds may be driven by large-scale atmospheric processes such as advection or may originate as coupled clouds that become decoupled after being lifted above the PBLH, and after the surface-driven thermals weaken or cease.

Compared with other regions, at the SGP and MAO, coupled conditions are associated with a deeper PBL and stronger sensible heat fluxes, indicating a more convective lower troposphere and an increased presence

of coupled cumulus clouds. In contrast, decoupled clouds, often detached from surface influences, occur in a shallow PBL with weaker heat fluxes and small diurnal variation, suggesting that their formation could be driven by large-scale atmospheric processes such as advection. At COR, is slightly higher for decoupled clouds in the morning and becomes slightly higher for coupled clouds in the afternoon. This may reflect a growing contribution from coupled cumulus clouds later in the day, though further investigation is needed to confirm this pattern. At FKB, PBLH differences between coupled and decoupled clouds are most pronounced in the afternoon, aligning with variations in sensible heat flux. Lastly, at TMP, coupled clouds exhibit a shallower PBLH than at other sites, pointing to weaker surface-driven turbulence and suggesting a dominant presence of stratiform clouds.

Although coupled and decoupled percentages are consistent across sites, different climatic and geographical configurations lead to observable differences in the coupled regime's peaking time and driving factors. The SGP site, characterized by wheat crops and grasslands, has a slow buildup of sensible heat flux and, hence, PBLH growth, causing coupled clouds to peak late in the afternoon. MAO, over the Amazon region, is highly influenced by strong convection and weak stratification, which facilitates the early uplifting of low-level clouds beyond the PBLH and causes coupled clouds to peak in the late morning. COR receives high moisture transported by the SALLJ at nighttime, which likely influences the formation of coupled stratocumulus clouds in the early morning. TMP and FKB, located in colder climates, are characterized by shallow boundary layers and probably coupled stratiform conditions. Seasonal variations at SGP highlight the influence of local thermal and moisture conditions on cloud coupling. Coupled clouds are more frequent in warmer seasons, particularly in spring (72.2% $\pm$ 9.6%), when enhanced surface heating and moisture transport promote cumulus cloud formation. In contrast, their occurrence decreases in fall (63.8% $\pm$ 14.1%), aligning with weaker convective conditions. The diurnal cycle of coupled clouds is most pronounced in spring and summer, peaking in the afternoon when surface heating is strongest. Meanwhile, decoupled clouds remain relatively stable across seasons, suggesting a weaker dependence on surface forcing. Sensible heat fluxes and PBLH variations further support this pattern, reinforcing the seasonal modulation of cloud coupling at SGP.

This study establishes a robust observational benchmark for cloud-surface coupling by documenting consistent coupling thresholds and occurrence patterns across diverse climatic and geographic regions. The relatively consistent coupling thresholds and occurrence rates observed at multiple sites could be beneficial for guiding future model evaluations or parameterization efforts. While further investigation is warranted, these findings mark a step toward improving the representation of cloud-surface interactions in weather and climate models. Furthermore, by underscoring the need for comprehensive observations and advanced methodologies, this research lays the groundwork for future investigations into the variability and evolution of low-level clouds across diverse climatic regions.

Conflict of Interest

The authors declare no conflicts of interest relevant to this study.

Data Availability Statement

All ARM data at five sites are publicly available at the USA Department of Energy Atmospheric Radiation Measurement Data Center: https://www.archive.arm.gov/discovery/. The planetary boundary layer height derived from DTDS over the Southern Great Plains can be downloaded from https://doi.org/10.5281/zenodo.7374849 (Su, 2022). The planetary boundary layer height for the ARM mobile facilities can be downloaded from https://zenodo.org/records/11061716 (Roldán-Henao & Su, 2024).

Acknowledgments

This work is supported in part by grants from the U.S. Department of Energy (DE-SC0022919) and the National Science Foundation (AGS2126098). YZ is supported by the DOE Early Career Grant (DE-SC0024185). T. Su is supported by the DOE Atmospheric System Research Science Focus Area THREAD project. Work at LLNL is performed under the auspices of the U.S. DOE by LLNL under Contract DE-AC52-07NA27344.

References

Albrecht, B. A., Bretherton, C. S., Johnson, D., Schubert, W. H., & Frisch, A. S. (1995). The Atlantic stratocumulus transition experiment—ASTEX. *Bulletin of the American Meteorological Society*, *76*(6), 889–904. https://doi.org/10.1175/1520-0477(1995)076<0889:TASTE>2.0.CO;2

Berg, L. K., Gustafson, W. I., Kassianov, E. I., & Deng, L. (2013). Evaluation of a modified scheme for shallow convection: Implementation of CuP and case studies. *Monthly Weather Review*, *141*(1), 134–147. https://doi.org/10.1175/MWR-D-12-00136.1

Berg, L. K., & Kassianov, E. I. (2008). Temporal variability of fair-weather cumulus statistics at the ACRF SGP site. *Journal of Climate*, *21*(13), 3344–3358. https://doi.org/10.1175/2007JCLI2266.1

Berg, L. K., & Stull, R. B. (2005). A simple parameterization coupling the convective daytime boundary layer and fair-weather cumuli. *Journal of the Atmospheric Sciences*, *62*(6), 1976–1988. https://doi.org/10.1175/JAS3437.1

Betts, A. K. (2009). Land-surface-atmosphere coupling in observations and models. *Journal of Advances in Modeling Earth Systems*, *1*(3). https://doi.org/10.3894/james.2009.1.4

Bretherton, C. S., Blossey, P. N., & Uchida, J. (2007). Cloud droplet sedimentation, entrainment efficiency, and subtropical stratocumulus albedo. *Geophysical Research Letters*, *34*(3), L03813. https://doi.org/10.1029/2006GL027648

Bretherton, C. S., & Wyant, M. C. (1997). Moisture transport, lower-tropospheric stability, and decoupling of cloud-topped boundary layers. *Journal of the Atmospheric Sciences*, *54*(1), 148–167. https://doi.org/10.1175/1520-0469(1997)054<0148:MTLTSA>2.0.CO;2

Cheruy, F., Dufresne, J. L., Hourdin, F., & Ducharne, A. (2014). Role of clouds and land-atmosphere coupling in midlatitude continental summer warm biases and climate change amplification in CMIP5 simulations. *Geophysical Research Letters*, *41*(18), 6493–6500. https://doi.org/10.1002/2014GL061145

Clothiaux, E. E., Ackerman, T. P., Mace, G. G., Moran, K. P., Marchand, R. T., Miller, M. A., & Martner, B. E. (2000). Objective determination of cloud heights and radar reflectivities using a combination of active remote sensors at the ARM CART sites. *Journal of Applied Meteorology*, *39*(5), 645–665. https://doi.org/10.1175/1520-0450(2000)039<0645:ODOCHA>2.0.CO;2

Dong, X., Schwantes, A. C., Xi, B., & Wu, P. (2015). Investigation of the marine boundary layer cloud and CCN properties under coupled and decoupled conditions over the Azores. *Journal of Geophysical Research*, *120*(12), 6179–6191. https://doi.org/10.1002/2014JD022939

Driedonks, A. G. M. (1982). Models and observations of the growth of the atmospheric boundary layer. *Boundary-Layer Meteorology*, *23*(3), 283–306. https://doi.org/10.1007/BF00121117

Ek, M. B., & Holtslag, A. A. M. (2004). Influence of soil moisture on boundary layer cloud development. *Journal of Hydrometeorology*, *5*(1), 86–99. https://doi.org/10.1175/1525-7541(2004)005<0086:IOSMOB>2.0.CO;2

Fast, J. D., Berg, L. K., Alexander, L., Bell, D., D'Ambro, E., Hubbe, J., et al. (2019). Overview of the HI-SCALE field campaign: A new perspective on shallow convective clouds. *Bulletin of the American Meteorological Society*, *100*(5), 821–840. https://doi.org/10.1175/bams-d-18-0030.1

Garratt, J. R. (1990). The internal boundary layer - A review. In *Boundary-Layer Meteorology* (Vol. 50(1–4), pp. 171–203). https://doi.org/10.1007/BF00120524

Glenn, I. B., Feingold, G., Gristey, J. J., & Yamaguchi, T. (2020). Quantification of the radiative effect of aerosol-cloud interactions in shallow continental cumulus clouds. *Journal of the Atmospheric Sciences*, *77*(8), 2905–2920. https://doi.org/10.1175/JAS-D-19-0269.1

Golaz, J. C., Larson, V. E., & Cotton, W. R. (2002). A PDF-based model for boundary layer clouds. Part I: Method and model description. *Journal of the Atmospheric Sciences*, *59*(24), 3540–3551. https://doi.org/10.1175/1520-0469(2002)059<3540:APBMFB>2.0.CO;2

Griesche, H. J., Ohneiser, K., Seifert, P., Radenz, M., Engelmann, R., & Ansmann, A. (2021). Contrasting ice formation in Arctic clouds: Surface-coupled vs. surface-decoupled clouds. *Atmospheric Chemistry and Physics*, *21*(13), 10357–10374. https://doi.org/10.5194/acp-21-10357-2021

Guo, J., Miao, Y., Zhang, Y., Liu, H., Li, Z., Zhang, W., et al. (2016). The climatology of planetary boundary layer height in China derived from radiosonde and reanalysis data. *Atmospheric Chemistry and Physics*, *16*(20), 13309–13319. https://doi.org/10.5194/acp-16-13309-2016

Guo, J., Zhang, J., Yang, K., Liao, H., Zhang, S., Huang, K., et al. (2021). Investigation of near-global daytime boundary layer height using high-resolution radiosondes: First results and comparison with ERA5, MERRA-2, JRA-55, and NCEP-2 reanalyses. *Atmospheric Chemistry and Physics*, *21*(22), 17079–17097. https://doi.org/10.5194/acp-21-17079-2021

Hogan, R. J., Grant, A. L. M., Illingworth, A. J., Pearson, G. N., & O'Connor, E. J. (2009). Vertical velocity variance and skewness in clear and cloud-topped boundary layers as revealed by Doppler lidar. *Quarterly Journal of the Royal Meteorological Society*, *135*(640), 635–643. https://doi.org/10.1002/qj.413

Jensen, M. P., & Del Genio, A. D. (2006). Factors limiting convective cloud-top height at the ARM Nauru Island climate research facility. *Journal of Climate*, *19*(10), 2105–2117. https://doi.org/10.1175/JCLI3722.1

Jensen, M. P., Petersen, W. A., Bansemer, A., Bharadwajwajwaj, N., Carey, L. D., Cecil, D. J., et al. (2016). The midlatitude continental convective clouds experiment (MC3E). *Bulletin of the American Meteorological Society*, *97*(9), 1667–1686. https://doi.org/10.1175/BAMS-D-14-00228.1

Jones, C. R., Bretherton, C. S., & Leon, D. (2011). Coupled vs. decoupled boundary layers in VOCALS-REx. *Atmospheric Chemistry and Physics*, *11*(14), 7143–7153. https://doi.org/10.5194/acp-11-7143-2011

Kollias, P., Bharadwaj, N., Clothiaux, E. E., Lamer, K., Oue, M., Hardin, J., et al. (2020). The ARM radar network: At the leading edge of cloud and precipitation observations. *Bulletin of the American Meteorological Society*, *101*(5), E588–E607. https://doi.org/10.1175/BAMS-D-18-0288.1

Lee, J. M., Zhang, Y., & Klein, S. A. (2019). The effect of land surface heterogeneity and background wind on shallow cumulus clouds and the transition to deeper convection. *Journal of the Atmospheric Sciences*, *76*(2), 401–419.

Liu, G., Liu, Y., & Endo, S. (2013). Evaluation of surface flux parameterizations with long-term ARM observations. *Monthly Weather Review*, *141*(2), 773–797. https://doi.org/10.1175/MWR-D-12-00095.1

Liu, S., & Liang, X. Z. (2010). Observed diurnal cycle climatology of planetary boundary layer height. *Journal of Climate*, *23*(21), 5790–5809. https://doi.org/10.1175/2010JCLI3552.1

Martin, S. T., Artaxo, P., MacHado, L. A. T., Manzi, A. O., Souza, R. A. F., Schumacher, C., et al. (2016). Introduction: Observations and modeling of the green ocean amazon (GoAmazon2014/5). *Atmospheric Chemistry and Physics*, *16*(8), 4785–4797. https://doi.org/10.5194/acp-16-4785-2016

Moeng, C. H., Cotton, W. R., Bretherton, C., Chlond, A., Khairoutdinov, M., Krueger, S., et al. (1996). Simulation of a stratocumulus-topped planetary boundary layer: Intercomparison among different numerical codes. *Bulletin of the American Meteorological Society*, *77*(2), 261–278. https://doi.org/10.1175/1520-0477(1996)077<0261:SOASTP>2.0.CO;2

Nicholls, S. (1984). The dynamics of stratocumulus: Aircraft observations and comparisons with a mixed layer model. *Quarterly Journal of the Royal Meteorological Society*, *110*(466), 783–820. https://doi.org/10.1002/qj.49711046603

Petäjä, T., O'Connor, E. J., Moisseev, D., Sinclair, V. A., Manninen, A. J., Väänänen, R., et al. (2016). BAECC: A field campaign to elucidate the impact of biogenic aerosols on clouds and climate. *Bulletin of the American Meteorological Society*, *97*(10), 1909–1928. https://doi.org/10.1175/BAMS-D-14-00199.1

Qian, Y., Huang, M., Yang, B., & Berg, L. K. (2013). A modeling study of irrigation effects on surface fluxes and land-air-cloud interactions in the southern Great Plains. *Journal of Hydrometeorology*, *14*(3), 700–721. https://doi.org/10.1175/JHM-D-12-0134.1

Roldán-Henao, N., & Su, T. (2024). Planetary boundary layer height retrievals from micropulse-lidar at four multiple ARM sites around the World (version 1) [Dataset]. *Zenodo*. https://doi.org/10.5281/zenodo.11061716

Roldán-Henao, N., Su, T., & Li, Z. (2024). Refining planetary boundary layer height retrievals from micropulse-lidar at multiple ARM sites around the world. *Journal of Geophysical Research: Atmospheres*, *129*(13), e2023JD040207. https://doi.org/10.1029/2023JD040207

Romps, D. M. (2017). Exact expression for the lifting condensation level. *Journal of the Atmospheric Sciences*, *74*(12), 3891–3900. https://doi.org/10.1175/JAS-D-17-0102.1

Santanello, J. A., Dirmeyer, P. A., Ferguson, C. R., Findell, K. L., Tawfik, A. B., Berg, A., et al. (2018). Land-atmosphere interactions the LoCo perspective. In *Bulletin of the American meteorological Society* (Vol. 99, pp. 1253–1272). https://doi.org/10.1175/BAMS-D-17-0001.1

Sisterson, D. L., Peppler, R. A., Cress, T. S., Lamb, P. J., & Turner, D. D. (2016). The ARM Southern Great Plains (SGP) site. *Meteorological Monographs*, *57*, 6.1–6.14. https://doi.org/10.1175/amsmonographs-d-16-0004.1

Song, F., Feng, Z., Ruby Leung, L., Houze, R. A., Wang, J., Hardin, J., & Homeyer, C. R. (2019). Contrasting Spring and summer large-scale environments associated with mesoscale convective systems over the U.S. Great Plains. *Journal of Climate*, *32*(20), 6749–6767. https://doi.org/10.1175/JCLI-D-18-0839.1

Stull, R. B. (1988). *An introduction to boundary layer meteorology* (Vol. 13). Springer Science & Business Media.

Su, T. (2022). Planetary boundary layer height (PBLH) over the SGP [Dataset]. *Zenodo*. https://doi.org/10.5281/zenodo.7374849

Su, T., Li, Z., Henao, N. R., Luan, Q., & Yu, F. (2024). Constraining effects of aerosol-cloud interaction by accounting for coupling between cloud and land surface. *Science Advances*, *10*(21), eadl5044. https://doi.org/10.1126/sciadv.adl5044

Su, T., Li, Z., & Kahn, R. (2020). A new method to retrieve the diurnal variability of planetary boundary layer height from LiDAR under different thermodynamic stability conditions. *Remote Sensing of Environment*, *237*, 111519. https://doi.org/10.1016/j.rse.2019.111519

Su, T., Li, Z., Zhang, Y., Zheng, Y., & Zhang, H. (2024). Observation and reanalysis derived relationships between cloud and land surface fluxes across cumulus and stratiform coupling over the Southern Great Plains. *Geophysical Research Letters*, *51*(8), e2023GL108090. https://doi.org/10.1029/2023GL108090

Su, T., Zhang, Y., & Tian, J. (2025). Boundary-layer-coupled and decoupled clouds in global storm-resolving models: Comparisons with the ARM observations. *Journal of Geophysical Research: Atmospheres*, *130*(5), e2024JD041915. https://doi.org/10.1029/2024jd041915

Su, T., Zheng, Y., & Li, Z. (2022). Methodology to determine the coupling of continental clouds with surface and boundary layer height under cloudy conditions from LiDAR and meteorological data. *Atmospheric Chemistry and Physics*, *22*(2), 1453–1466. https://doi.org/10.5194/acp-22-1453-2022

Tang, S., Xie, S., Zhang, M., Tang, Q., Zhang, Y., Klein, S. A., et al. (2019). Differences in eddy-correlation and energy-balance surface turbulent heat flux measurements and their impacts on the large-scale forcing fields at the ARM SGP site. *Journal of Geophysical Research: Atmospheres*, *124*(6), 3301–3318. https://doi.org/10.1029/2018JD029689

Tao, C., Zhang, Y., Tang, S., Tang, Q., Ma, H. Y., Xie, S., & Zhang, M. (2019). Regional moisture budget and land-atmosphere coupling over the US Southern Great Plains inferred from the ARM long-term observations. *Journal of Geophysical Research: Atmospheres*, *124*(17–18), 10091–10108. https://doi.org/10.1029/2019jd030585

Teixeira, J., & Hogan, T. F. (2002). Boundary layer clouds in a global atmospheric model: Simple cloud cover parameterizations. *Journal of Climate*, *15*(11), 1261–1276. https://doi.org/10.1175/1520-0442(2002)015<1261:BLCIAG>2.0.CO;2

Tian, J., Zhang, Y., Klein, S. A., Öktem, R., & Wang, L. (2022). How does land cover and its heterogeneity length scales affect the formation of summertime shallow cumulus clouds in observations from the US Southern Great Plains? *Geophysical Research Letters*, *49*(7), e2021GL097070. https://doi.org/10.1029/2021GL097070

Turton, J. D., & Nicholls, S. (1987). A study of the diurnal variation of stratocumulus using a multiple mixed layer model. *Quarterly Journal of the Royal Meteorological Society*, *113*(477), 969–1009. https://doi.org/10.1002/qj.49711347712

Twine, T. E., Kustas, W. P., Norman, J. M., Cook, D. R., Houser, P., Meyers, T. P., et al. (2000). Correcting eddy-covariance flux underestimates over a grassland. *Agricultural and Forest Meteorology*, *103*(3), 279–300. https://doi.org/10.1016/s0168-1923(00)00123-4

Varble, A. C., Nesbitt, S. W., Salio, P., Hardin, J. C., Bharadwaj, N., Borque, P., et al. (2021). Utilizing a storm-generating hotspot to study convective cloud transitions: The CACTI experiment. *Bulletin of the American Meteorological Society*, *102*(8), E1597–E1620. https://doi.org/10.1175/BAMS-D-20-0030.1

Vogelezang, D. H. P., & Holtslag, A. A. M. (1996). Evaluation and model impacts of alternative boundary-layer height formulations. *Boundary-Layer Meteorology*, *81*(3–4), 245–269. https://doi.org/10.1007/BF02430331

Wang, K., & Dickinson, R. E. (2012). A review of global terrestrial evapotranspiration: Observation, modeling, climatology, and climatic variability. *Reviews of Geophysics*, *50*(2). https://doi.org/10.1029/2011rg000373

Wood, R. (2012). Stratocumulus clouds. In *Monthly Weather Review* (Vol. 140(8), pp. 2373–2423). https://doi.org/10.1175/MWR-D-11-00121.1

Wu, X., Grabowski, W. W., & Moncreff, M. W. (1998). Long-term behavior of cloud systems in TOGA COARE and their interactions with radiative and surface processes. Part I: Two-dimensional modeling study. *Journal of the Atmospheric Sciences*, *55*(17), 2693–2714. https://doi.org/10.1175/1520-0469(1998)055<2693:LTBOCS>2.0.CO;2

Wulfmeyer, V., Behrendt, A., Kottmeier, C., Corsmeier, U., Barthlott, C., Craig, G. C., et al. (2011). The convective and Orographically-induced precipitation study (COPS): The scientific strategy, the field phase, and research highlights. *Quarterly Journal of the Royal Meteorological Society*, *137*(1), 3–30. https://doi.org/10.1002/qj.752

Wyant, M. C., Bretherton, C. S., Rand, H. A., & Stevens, D. E. (1997). Numerical simulations and a conceptual model of the stratocumulus to trade cumulus transition. *Journal of the Atmospheric Sciences*, *54*(1), 168–192. https://doi.org/10.1175/1520-0469(1997)054<0168:NSAACM>2.0.CO;2

Xian, T., Guo, J., Zhao, R., Su, T., & Li, Z. (2023). The impact of urbanization on mesoscale convective systems in the Yangtze River Delta region of China: Insights gained from observations and modeling. *Journal of Geophysical Research: Atmospheres*, *128*(3), e2022JD037709. https://doi.org/10.1029/2022jd037709

Xie, S., McCoy, R. B., Klein, S. A., Cederwall, R. T., Wiscombe, W. J., Clothiaux, E. E., et al. (2010). Clouds and more: ARM climate modeling best estimate data: A new data product for climate studies. *Bulletin of the American Meteorological Society*, *91*(LLNL-JRNL-412676), 13–20. https://doi.org/10.1175/2009bams2891.1

Zhang, H., Su, T., Zheng, Y., & Li, Z. (2024). First assessment of cloud-land coupling in LASSO large-eddy simulations. *Geophysical Research Letters*, *51*(14), e2024GL109774. https://doi.org/10.1029/2024gl109774

Zhang, Y., Klein, S. A., Fan, J., Chandra, A. S., Kollias, P., Xie, S., & Tang, S. (2017). Large-eddy simulation of shallow cumulus over land: A composite case based on ARM long-term observations at its Southern Great Plains site. *Journal of the Atmospheric Sciences*, *74*(10), 3229–3251. https://doi.org/10.1175/JAS-D-16-0317.1

Zheng, Y., & Li, Z. (2019). Episodes of warm-air advection causing cloud-surface decoupling during the MARCUS. *Journal of Geophysical Research: Atmospheres*, *124*(22), 12227–12243. https://doi.org/10.1029/2019JD030835

Zheng, Y., & Rosenfeld, D. (2015). Linear relation between convective cloud base height and updrafts and application to satellite retrievals. *Geophysical Research Letters*, *42*(15), 6485–6491. https://doi.org/10.1002/2015GL064809

Zheng, Y., Rosenfeld, D., & Li, Z. (2018a). Estimating the decoupling degree of subtropical marine stratocumulus decks from satellite. *Geophysical Research Letters*, *45*(22). https://doi.org/10.1029/2018GL078382

Zheng, Y., Rosenfeld, D., & Li, Z. (2018b). The relationships between cloud top radiative cooling rates, surface latent heat fluxes, and cloud-base heights in marine stratocumulus. *Journal of Geophysical Research: Atmospheres*, *123*(20). https://doi.org/10.1029/2018JD028579

Zheng, Y., Sakradzija, M., Lee, S. S., & Li, Z. (2020). Theoretical understanding of the linear relationship between convective updrafts and cloud-base height for shallow cumulus clouds. Part II: Continental conditions. *Journal of the Atmospheric Sciences*, *77*(4), 1313–1328. https://doi.org/10.1175/JAS-D-19-0301.1

Zheng, Y., Zhang, H., & Li, Z. (2021). Role of surface latent heat flux in shallow cloud transitions: A mechanism-denial les study. *Journal of the Atmospheric Sciences*, *78*(9). https://doi.org/10.1175/JAS-D-20-0381.1